

An all-joint-control master device for single-port laparoscopic surgery robots

Seongbo Shim¹ · Taehun Kang³ · Daekeun Ji¹ ·
Hyunseok Choi¹ · Sanghyun Joung² · Jaesung Hong¹

Received: 18 July 2015 / Accepted: 14 January 2016 / Published online: 12 February 2016
© CARS 2016

Abstract

Purpose Robots for single-port laparoscopic surgery (SPLS) typically have all of their joints located inside abdomen during surgery, whereas with the da Vinci system, only the tip part of the robot arm is inserted and manipulated. A typical master device that controls only the tip with six degrees of freedom (DOFs) is not suitable for use with SPLS robots because of safety concerns.

Methods We designed an ergonomic six-DOF master device that can control all of the joints of an SPLS robot. We matched each joint of the master, the slave, and the human arm to decouple all-joint motions of the slave robot. Counterbalance masses were used to reduce operator fatigue. Mapping factors were determined based on kinematic analysis and were used to achieve all-joint control with minimal error at the tip of the slave robot.

Results The proposed master device has two noteworthy features: efficient joint matching to the human arm to decouple each joint motion of the slave robot and accurate mapping factors, which can minimize the trajectory error of the tips between the master and the slave.

Conclusions We confirmed that the operator can manipulate the slave robot intuitively with the master device

and that both tips have similar trajectories with minimal error.

Keywords Single-port laparoscopic surgery robot · Master device · All-joint control · Mapping factor

Introduction

Single-port laparoscopic surgery (SPLS) makes use of the navel as an entry point for surgical tools. Because of the creation of a single incision around the navel, SPLS results in less postoperative scarring, less postoperative pain, and more rapid recovery than conventional open surgery or multi-port laparoscopic surgery [1]. However, because the surgical instruments are intersected through the navel, the operation is counterintuitive and difficult [2], and a significant amount of training is required. In addition, high levels of concentration are required to manipulate the instruments appropriately [3–5].

To overcome these technical difficulties, master–slave robot systems have been developed. Surgeons can control the slave surgical robot by manipulating a master device at a remote location [6, 7]. When the surgeon manipulates the master device while watching the endoscopic image, the master device records the position and orientation of the surgeon's hands. After calculating the corresponding motion, the slave robot moves to perform the surgery. A typical example of a master–slave system is the da Vinci surgical system [8]. Using such robotic systems, surgeons can focus on the surgery using the master device, without considering the structure of the slave robot. If necessary, this type of master device can switch the control mode between left and right, adjusted to the counterintuitive configuration of the slave robot. There have been a number of reports of studies

✉ Jaesung Hong
jhong@dgist.ac.kr

¹ Department of Robotics Engineering, DGIST,
333, Techno jungang-daero, Hyeonpung-myeon,
Dalseong-gun, Daegu, Korea

² Medical Device and Robot Institute of Park,
Kyungpook National University, 80 Daehakro, Bukgu,
Daegu 702-701, Korea

³ Division of IoT & Robotics Convergence Research, DGIST,
333, Techno jungang-daero, Hyeonpung-myeon,
Dalseong-gun, Daegu, Korea

on slave robots for SPLS but relatively few reports of studies on master devices. In this study, we focused on a master device for SPLS slave robots.

When designing a master device for an SPLS robot, it is necessary to note the structural differences between multi-port surgical robots, such as the da Vinci system in which most of the joints are outside the body during surgery, and SPLS robots in which most of the joints are located inside the abdominal cavity. In SPLS robots, following insertion through a single entry point, the robot spreads its arms and takes an appropriate pose for the surgery using multiple joints [9–11]. A robot that spreads in this manner after insertion is referred to as a Y-type robot, as the robot forms a “Y” shape (see Fig. 1b).

On the other hand, master devices for robot control can be separated into two types. Devices of the first type are tip-control master devices that control only the tip of the slave robot by calculating the change in the rotation and translation of the tip in a Cartesian space. Most master devices use such a tip-control method, including the da Vinci system [9], the PHANTOM OMNI system [10], and the DLR MiroSurge robot [11]. Because a tip-control master device allows the tip of the slave robot to follow the tip of the master device, the user can manipulate the slave robot intuitively. This type of master device is commonly used for both general-purpose applications and surgical applications.

Devices of the second type are all-joint-control master devices that manipulate not only the tip but also the intermediate joints of the slave robot, using a joint-to-joint mapping technique. Using tip control, the motion of each joint cannot be monitored precisely. However, in a Y-type slave robot for SPLS, most of the joints of the robot are located in the body; therefore, all of the joints, including the tip, should be operated within safe limits or intended workspace. If we use tip control, some unmonitored intermediate joint motion may result in damage to tissue; therefore, all-joint control is preferable. All-joint control is performed for each joint

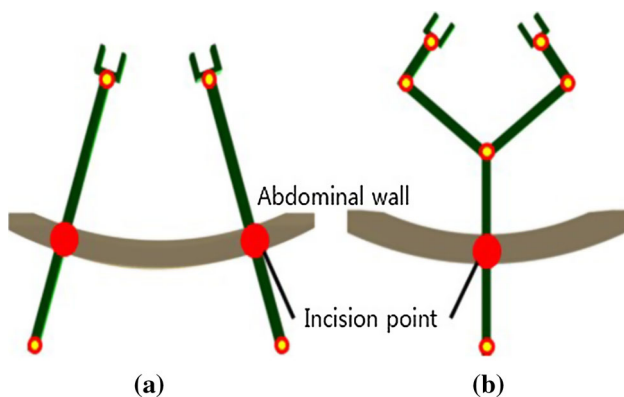


Fig. 1 Laparoscopic surgery robots. **a** Multi-port surgery robot and **b** single-port surgery robot

space, in contrast to tip control in an integrated single Cartesian space. An example of the all-joint control method is the master–slave Mutual Telexistence system [12], in which the operator can easily manipulate a specific joint of the slave robot via joint-linking motions of the master and the slave. However, this is for a slave robot which has the same structure as a human arm for non-medical purpose.

In the field of surgical robots, all-joint control has been applied to several master devices. Hyper Finger [13] is a compact and lightweight robotic system for minimally invasive surgery that has nine degrees of freedom (DOFs). However, because not every joint of the master device is matched to one of the human arm, the joints of the slave robot cannot be manipulated separately. A flexible endoscopic gastrointestinal robot manipulator has also been proposed [14]. Although this provides total joint matching, the wearable exoskeleton leads to fatigue owing to its weight. MASTER, proposed by Phee et al. [15], allows the end effector to mimic the motion of the master device, but the master device has only three rotational joints. The prismatic joints of the slave robot must be manipulated separately using a footswitch. To the best of our knowledge, there is no master device that can control all of the joints of a six-DOF surgical robot separately.

In this paper, we describe the development of a new six-DOF master device for SPLS robots that supports all-joint control. The master was primarily designed for the PLAS robot [16], which is a Y-type slave device developed by the author group. Although the master was initially designed for PLAS, the design concept of the master device may be applied to other SPLS robots with appropriate modifications. Most SPLS robot arms should be articulated inside the body to make the triangulation layout with an endoscope. The proposed master device efficiently matches the human wrist and elbow to the SPLS robot joints inside the body.

We designed the master device to decouple all-joint motions of the slave robot with considering operator ergonomics. Joint matching between the slave, the master, and the human arm should be analyzed, considering the range of motion of the human arm [17, 18]. We confirmed that each joint motion of the slave robot is well decoupled using the proposed master device.

Furthermore, we identified optimal mapping factors between the master and slave robots based on a velocity matching algorithm. The master and slave have different joint structures; therefore, a simple 1:1 joint mapping leads to velocity differences. An inverse Jacobian method was not used because of coupling motions of the joints; instead, we used kinematics analysis to identify appropriate mapping factors that minimize the velocity error. We performed simulations to assess the correctness of the mapping factors.

The main contribution of this study is the development of a new six-DOF master device for all-joint control of SPLS robots with optimized mapping factors.

Design of all-joint matching master device

With a tip-control master device, only the motion at the end effector of the slave robot is important. However, with an all-joint-control master device, not only the end effector but also all of the other joints of the slave robot should be matched to the corresponding joints of the master device.

To design the master device, we investigated the structures of the joints of the slave robot and those of the human arm. If we were to consider only the structure of the slave robot and were to build a master device that mimics this motion, the structure of the master would differ from that of the human arm, which would limit the natural motion of the arm.

The range of joint angle of the master device was determined based on the analysis of human arm joints by Wang et al. [17]. The wrist rotates from -70° to $+60^\circ$ in flexion/extension and from 0° to 50° in abduction/adduction. The angle of flexion of the elbow joint is 142° , and those of supination/pronation are up to 90° and 80° , respectively. The master device was designed considering these ergonomic factors, as well as counterbalance masses to minimize operator fatigue [19].

Structure of the slave robot

The partner slave robot for the proposed master is the PLAS robot [16], although the proposed master is not limited to use with this slave robot. It is difficult to produce sufficient torque to operate on relatively large organs, such as the intestines and liver, using SPLS robots. With the PLAS robot, a plate-spring mechanism is used to produce a large force. The PLAS robot has six DOFs for each of the arms, which consist of two prismatic joints (joints 1 and 5) and four rotational joints (joints 2, 3, 4, and 6), as shown in Fig. 2. Joint 1 provides a large workspace by separating the starting point for each arm; joints 2 and 3 are used to create a yaw angle; and joints 4 and 6 correspond to pitch and roll, respectively. Joint 5 creates forward and backward motion, once the orientation has been determined. We considered all DOFs of the individual arms, resulting in a total of 12 DOFs for the design. Because all of the joints of the PLAS robot are located inside abdomen, all-joint-control of the master device should be used.

Design of all-joint-control master device

To manipulate the PLAS robot using all-joint control, the master device requires two yaw axes, one pitch axis, one roll axis, and two prismatic joints. To control each joint of the slave robot separately, all joints of the master device must be decoupled. Matching between the master device and the human arm to decouple the six DOFs of the slave robot is achieved by assigning one yaw axis to the elbow and pitch, roll, and the other yaw axis to the wrist. One prismatic joint

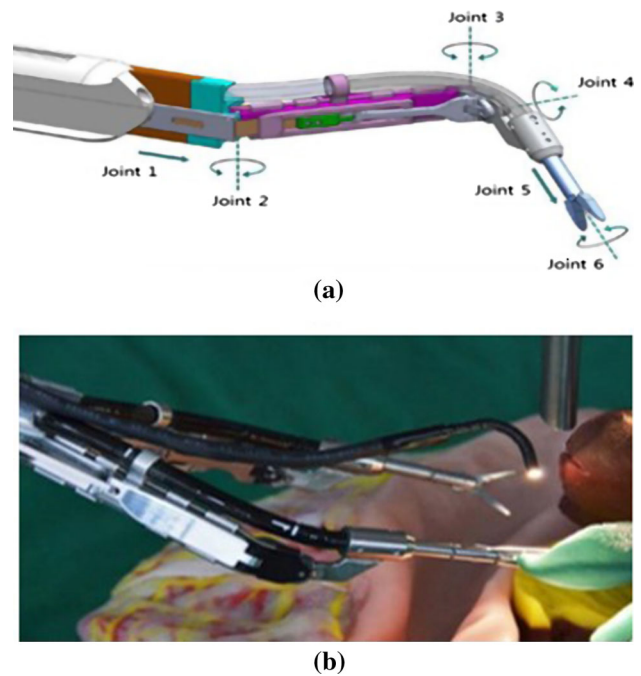


Fig. 2 The PLAS slave robot for the proposed master. **a** CAD model and **b** prototype [16]

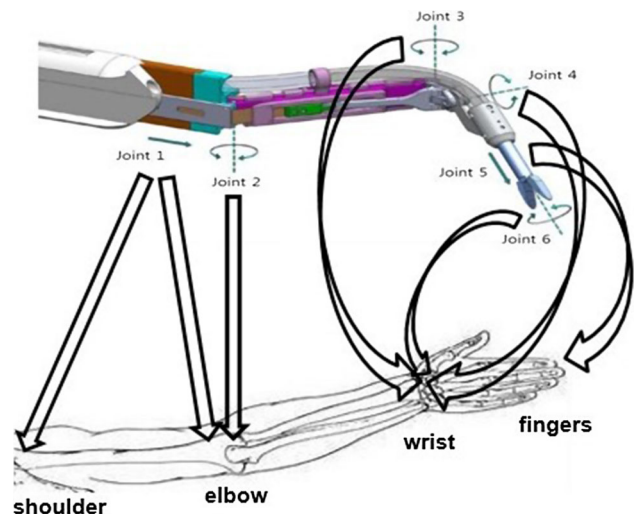


Fig. 3 Joint matching between the slave robot and the human arm

of the master device is matched to the linear motion of human forearm composed by the rotations of the shoulder and elbow. Another prismatic joint is matched to linear motions of the fingers, as shown in Fig. 3.

We designed a master device to implement matching between the human arm and the PLAS robot described above (see Fig. 4). Joint 2 of the master device (which is matched to the elbow) is related to joint 2 of the slave robot. The joint is also an armrest that supports the weight of the operator's arm. Joints 3, 4, and 5 of the master device (which are rotated by the wrist) correspond to joints 3, 4, and 6 of the

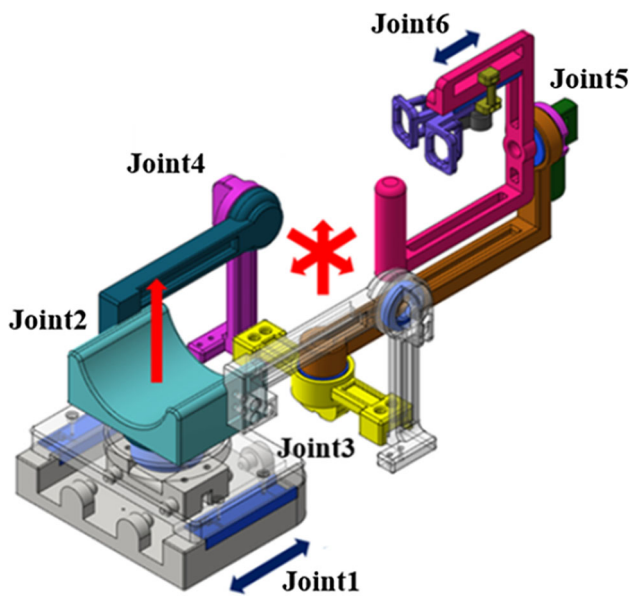


Fig. 4 CAD model of the proposed master device

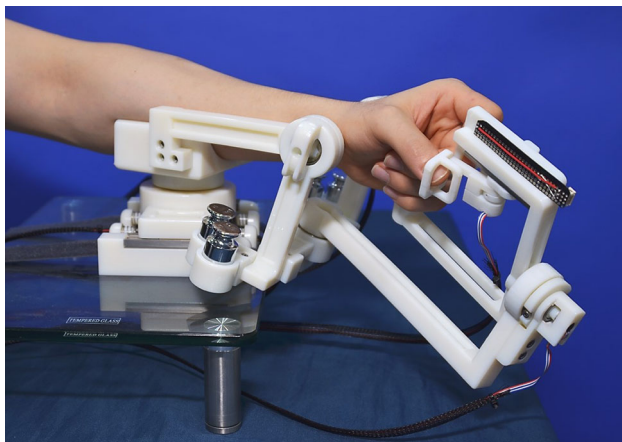


Fig. 5 A prototype of the proposed master device

slave robot. By matching these rotational joints to the wrist joint appropriately, the total amount of motion required for manipulation is reduced, thus reducing operator fatigue. Joint 1 of the master device matched to joint 1 of the slave robot translates in response to linear motion of the forearm through the rotations of the shoulder and elbow. Joint 6 of the master device is controlled by translation of the fingers and is matched to joint 5 of the slave robot. This matching permits manipulation of overall and fine translation movement separately using the forearm and the fingers. Figure 5 shows a photograph of the prototype master device.

Balance of the positioning stage

Because of the mass of the links after joint 4, it is difficult to rotate joint 4 in response to pitch rotation of the wrist. The

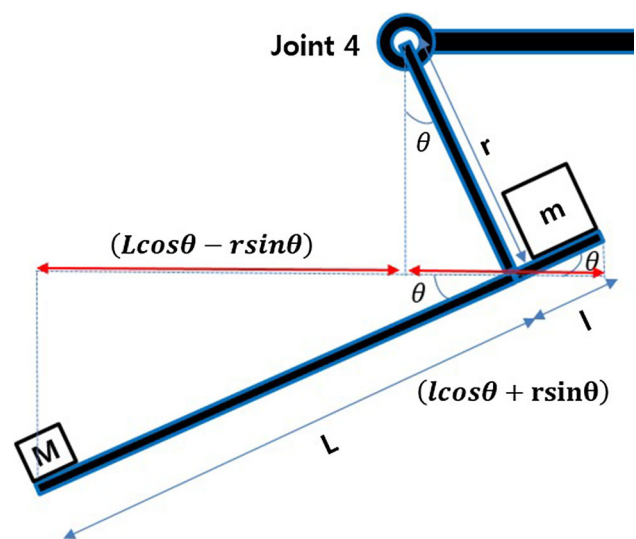


Fig. 6 Schematic diagram of the positioning of joint 4

mass of the links after joint 4 is approximately 240 g, and the joint is tilted by approximately 60°. Considering that the wrist is rotated from 0° to 50° on average in abduction/adduction, the operator should withstand the weight associated with it, which may result in fatigue during long surgical operations. To limit operator fatigue, joint 4 should be tilted to approximately 25° in the steady state.

To obtain a joint angle of 25° for joint 4 in the steady state, the master device contains two counterbalance masses on either side, as shown in Fig. 6. The values of the parameters shown in Fig. 6 are as follows: $r = 9$ cm, $M = 240.5$ g, $L = 18.8$ cm, and $l = 3.4$ cm. Using the following relations between the positioning stage, we may determine the mass m :

$$2m (r \sin \theta + l \cos \theta) = M (L \cos \theta - r \sin \theta), \tag{1}$$

$$2m = \frac{M (L \cos \theta - r \sin \theta)}{(r \sin \theta + l \cos \theta)}. \tag{2}$$

We find that $2m = 460$ g. By placing 230 g counterbalancing masses on both sides of the joint, joint 4 can be tilted by 25°, as shown in Fig. 7.

Sensors and materials

Sensors are required to measure the motion of the master device, and the number of sensors should be equal to the number of joints. The master device consists of two prismatic joints and four rotational joints. The motion of joint 1 is detected using two XSS-5GL13 on/off push switches (Zhejiang Xurui Electronic Co., Wenzhou, China) because the stroke of joint 1 of the slave robot is too long to be controlled using one-to-one motion matching. When an external force does not act on joint 1, the joint maintains the center of displacement due to the elastic force of springs mounted



Fig. 7 The angle of joint 4 with the counterbalance masses

on each side. When joint 1 is moved forward or backward, a switch is pushed and generates a signal. Rotational motions of joints 2 to 5 are detected using Ultra Miniature Encoder 7S series sensors (Nemicon Corp., Tokyo, Japan). These devices have a high angular resolution of approximately 0.225° , a diameter of 7.2 mm, and a height of 13.5 mm. The mass of the encoder is approximately 5 g, enabling easy manipulation of the master device. Joint 6 uses a linear potentiometer (PTL45-15R0-103B2, Bourns Inc., Altadena, CA) for linear motion instead of an encoder. The potentiometer has a resistance of 10 k Ω , and it is approximately 60 mm long, 9 mm wide, and 7 mm high.

All of the components of the master device were fabricated with a rapid prototyping machine (Eden 250TM, Stratasys Ltd., Rehovot, Israel). The machine has a resolution of 16 μ m, and the material used was FullCure 835 (Stratasys Ltd., Rehovot, Israel), which has a tensile strength of 57 MPa and a minimum elastic modulus of 2220 MPa. This material is sufficiently strong to manipulate the master device using a human arm. In addition, the rotational and prismatic joints were equipped with bearings and linear guides to minimize friction.

Master–slave mapping

The structure of the master device differs from that of the slave, the PLAS robot, because of the ergonomics of the human arm. Because of these differences, simple one-to-one mapping would lead to velocity and positional errors at the tip. The inverse Jacobian [20] is given by the following relations:

$$v_M = J_M \Theta'_M, \tag{3}$$

$$v_S = J_S \Theta'_S, \tag{4}$$

where v_M , J_M , and Θ'_M represent Cartesian velocity, Jacobian, and joint velocity of the master device, and v_S , J_S , and Θ'_S represent the corresponding properties of the slave robot. To have the same Cartesian velocity between master and slave, the joint velocity of the slave robot is determined as follows:

$$\Theta'_S = J_S^{-1} v_S, \tag{5}$$

$$\Theta'_S = J_S^{-1} v_M = J_S^{-1} J_M \Theta'_M. \tag{6}$$

A Jacobian-based approach is widely used to ensure that the velocity at the tip of the slave robot is equal to that at the tip of the master device. However, it is not straightforward to apply this method to all-joint-control master devices, such as that described here. Some joints have coupled motion; therefore, we may confine the tip motion but not confine the motion of each joint separately. There is thus a risk that the motion of some joints may damage organs or tissue during surgery.

We identified mapping factors that permit one-to-one joint control with minimal error at the tip. To determine these mapping factors for each joint, the kinematics of the master device were analyzed, as described in the following subsection.

Kinematics of the master device

Figure 8 shows a kinematic representation of the master device. The axes are labeled according to the distal Denavit–Hartenberg (D–H) convention [21], and the corresponding D–H parameters are listed in Table 1. Joints 1 and 6 are prismatic joints, and joints 2, 3, 4, and 5 are rotational joints. In Fig. 8, d_1 represents translation of the forearm; d_6 represents translation of the fingers; and θ_2 , θ_3 , θ_4 , and θ_5 are the angles of the elbow, yaw, pitch, and roll of the wrist, respectively. The value of d_1 is increased in proportion to the length of time that the switch is pushed. The dimensions shown in

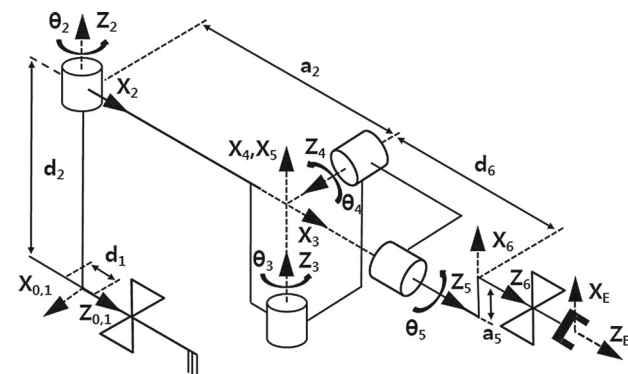


Fig. 8 Kinematic model of the master device. The axes are labeled according to the distal Denavit–Hartenberg convention

Table 1 D–H parameters of the master device

| Joint i | α_{i-1} | a_{i-1} | d_i | θ_i |
|-----------|-----------------|-----------|-------------------------------|--|
| 1 | 0 | 0 | $d_1 = \text{variable}$ | 0 |
| 2 | $\frac{\pi}{2}$ | 0 | d_2 | $\theta_2 = \text{variable} + \frac{\pi}{2}$ |
| 3 | 0 | a_2 | 0 | $\theta_3 = \text{variable}$ |
| 4 | $\frac{\pi}{2}$ | 0 | 0 | $\theta_4 = \text{variable} + \frac{\pi}{2}$ |
| 5 | $\frac{\pi}{2}$ | 0 | 0 | $\theta_5 = \text{variable}$ |
| 6 | 0 | a_5 | $d_6 = \text{variable} + d_6$ | 0 |

Fig. 8 are as follows: $d_2 = 88 \text{ mm}$, $a_2 = 138 \text{ mm}$, $a_5 = 45 \text{ mm}$, and $d_6 = 110 \text{ mm}$.

Mapping factors for decoupling all joints

The mapping factors for the four revolute joints were determined as follows. Because joint 1 is moved using an on/off switching mode and joint 6 is moved forward and backward after the orientation is determined, the prismatic joints were considered independently from the rotational joints. The mapping factors for the rotational joints were considered to produce similar trajectories of the master and the slave. Because the structure of the master differs from that of the slave, there will inevitably be differences in the velocities and trajectories of the tips if we use all-joint control. We attempted to minimize these differences and to match the velocity and trajectory as closely as possible between the master and slave, while maintaining joint-to-joint control.

To obtain the mapping factors for the rotational joints, kinematic models of the master and slave were modified from six DOFs to four DOFs by excluding the two prismatic joints, as shown in Fig. 9. By multiplying link-transformation matrices of the master and the slave, each total transformation matrix that relates the base frame to the end frame is calculated [21]. Jacobian matrices are derived by performing partial differentiation of the total transformation matrices

with respect to joint variables [20]. The Jacobian of the simplified slave robot J_S is given by

$$\begin{bmatrix} (-S_{23}(a_3 + d_5C_4) - a_2S_2) & (-S_{23}(a_3 + d_5C_4)) & (-d_5S_4C_{23}) \\ (C_{23}(a_3 + d_5C_4) + a_2C_2) & (C_{23}(a_3 + d_5C_4)) & (-d_5S_4S_{23}) \\ 0 & 0 & (d_5C_4) \end{bmatrix},$$

where S_{xy} represents $\sin(x + y)$. And the Jacobian of the simplified master device J_M is defined by

$$\begin{bmatrix} (-S_{23}(d_6C_4) - a'_2S_2) & (-S_{23}(d_6C_4)) & (-d_6S_4C_{23}) \\ (C_{23}(d_6C_4) + a'_2C_2) & (C_{23}(d_6C_4)) & (-d_6S_4S_{23}) \\ 0 & 0 & (d_6C_4) \end{bmatrix}$$

The constants in these expressions are as follows: $a_2 = 50$, $a_3 = 15$, $d_5 = 30$, $a'_2 = 138$, and $d_6 = 60$.

To achieve all-joint control, we assumed $\theta'_{Si} = K_i * \theta'_{Mi}$; that is, each joint of the slave robot was assumed to be actuated in response to motion of the corresponding joint of the master device. Using Eqs. (3) and (4), a diagonal matrix K was constructed as follows:

$$v_S = v_M, \tag{7}$$

$$J_S \theta'_S = J_M \theta'_M, \tag{8}$$

$$J_S K * \theta'_M = J_M \theta'_M. \tag{9}$$

$$J_S \begin{bmatrix} K_2 & 0 & 0 \\ 0 & K_3 & 0 \\ 0 & 0 & K_4 \end{bmatrix} = J_M. \tag{10}$$

Using the third-row vector of Eq. (10), the term K_4 may be obtained as follows:

$$(d_5C_4) K_4 = (d_6C_4), \quad K_4 = \frac{d_6}{d_5}. \tag{11}$$

K_3 may then be calculated from the second-row vector of Eq. (10), i.e.,

Fig. 9 Kinematic model of the rotational joints. **a** PLAS slave robot and **b** the master device

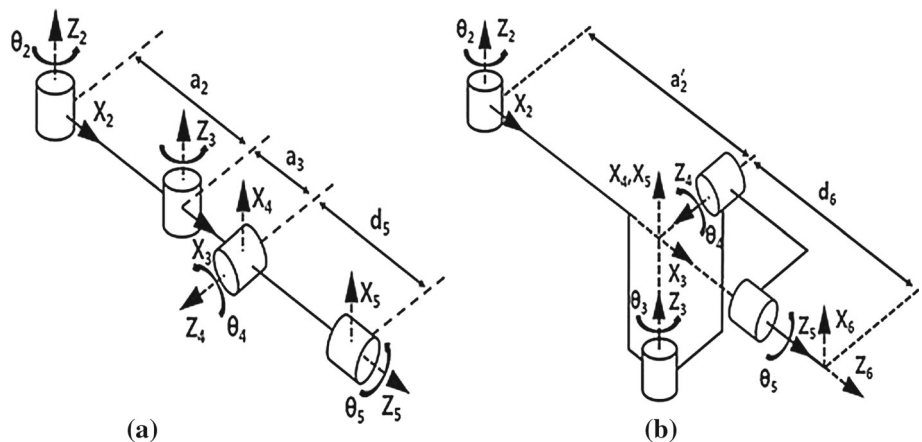


Table 2 Mapping factors between master and slave

| Joint <i>i</i> | Mapping factor |
|----------------|--|
| 1 | On/Off |
| 2 | $\frac{(C_{23}(d_6C_4)+a'_2C_2)}{(C_{23}(a_3+d_5C_4)+a_2C_2)}$ |
| 3 | $\frac{(d_6C_4)}{(a_3+d_5C_4)}$ |
| 4 | $\frac{(d_6)}{(d_5)}$ |
| 5 | 1 |
| 6 | 1 |

$$(C_{23}(a_3 + d_5C_4)) K_3 = (C_{23}(d_6C_4)),$$

$$K_3 = \frac{(d_6C_4)}{(a_3 + d_5C_4)}. \tag{12}$$

K_2 can be calculated using the second-row vector of Eq. (10), i.e.,

$$(C_{23}(a_3 + d_5C_4) + a_2C_2) K_2 = (C_{23}(d_6C_4) + a'_2C_2),$$

$$K_2 = \frac{(C_{23}(d_6C_4) + a'_2C_2)}{(C_{23}(a_3 + d_5C_4) + a_2C_2)}. \tag{13}$$

The first-, second-, and third-row vectors of Eq. (10) are related to v_x , v_y , and v_z , respectively. The mapping factors are listed in Table 2.

Although the master and slave have similar velocities because of the use of these mapping factors, errors in the velocities and resulting trajectories at the tips cannot be avoided using all-joint control. When the mapping factors in Eq. (10) were used, the velocity components v_y and v_z of the master and slave were equal. However, there was inevitable error in v_x , i.e.,

$$J_S K - J_M = (S_23(d_6C_4) + a'_2S_2) \frac{(C_{23}(d_6C_4) + a'_2C_2)}{(C_{23}(a_3 + d_5C_4) + a_2C_2)} \times (S_23(a_3 + d_5C_4) + a_2S_2). \tag{14}$$

Since the operation times of the master and the slave are identical, this error in velocity results in the final trajectory error between the master and the slave as shown in Fig. 15, which is considered acceptable for the task of handling tissue.

Experiment and results

To evaluate the performance of the system, we connected the master device and the slave robot and performed basic translation, rotation, and grasping tasks. We also verified the mapping factors via simulations. We confirmed that each slave joint was controlled without coupling to the corresponding master joint using the mapping factors. To assess

the error at the tip, the trajectories of the master and slave tips were compared using simulations.

Decoupling each joint motion of the slave robot

Using the master device, the slave robot was manipulated as shown in Fig. 10. When the elbow was folded, joint 2 of the robot rotated. When the wrist was rotated in the order of yaw, pitch, and roll, joints 3, 4, and 6 were rotated in sequence. When the forearm and fingers were translated, joints 1 and 5 moved forward and backward. These results confirm that each joint of the slave robot can be controlled separately using the master device. We also obtained some feedback from users. First, because of the armrest (joint 2), they were able to manipulate the master device without a significant burden. Second, because the master device matched each joint of the human arm and the slave robot, each joint motion of the slave robot could be decoupled.

Evaluation of the mapping factors

We investigated whether the tips of the master and the slave had similar trajectories using the rotational joints. Using the mapping factors listed in Table 2, we plotted the trajectories of the master and the slave using MATLAB (MathWorks Inc., Natick, MA). To evaluate only the performance of each mapping factor without physical errors, we used simulation instead of the physical prototype. When the master device rotated through 30° at joint 2, the slave robot rotated by 62.5° at the same joint using the mapping factors listed in Table 2. As a result, both tips moved 103.6 mm, as shown in Fig. 11. When joint 3 of the master device rotated through 30°, joint 3 of the slave rotated by 40° using the corresponding mapping factor. As a result, we found that the mapping factor allowed for motion of 31.4 mm of both tips, as shown in Fig. 12. With joint 4, we were able to obtain identical motion of both tips with zero error using the mapping factors, as shown in Fig. 13. Note that this complete agreement between master and slave occurred only when the remaining joints were stationary. When the joints moved in combination, some error occurred at the tip (as described later).

Trajectory error with the master device

We carried out simulations using the VTK graphic library (Kitware Inc., Clifton Park, NY) to characterize the relationship between the trajectories of the master and slave robot tips. We used the master device, a virtual slave system, and a 2560 Arduino Mega controller (Arduino Corp., Ivrea, Italy) to connect them, as shown in Fig. 14. A virtual slave robot was simulated based on the mechanical drawings and 3D model of the slave robot, PLAS, to evaluate the performance of the master device and the accuracy of mapping factors,

Fig. 10 Motion of the rotational joints of the master and slave

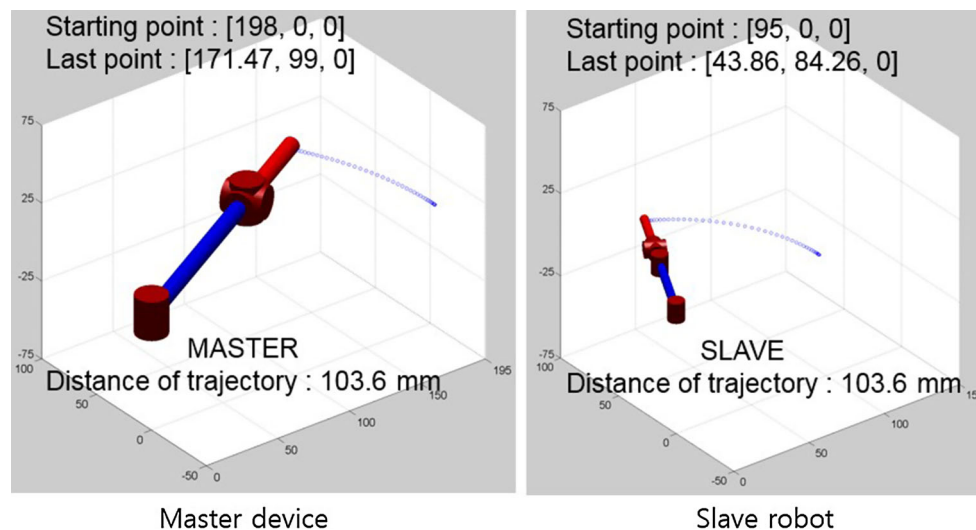
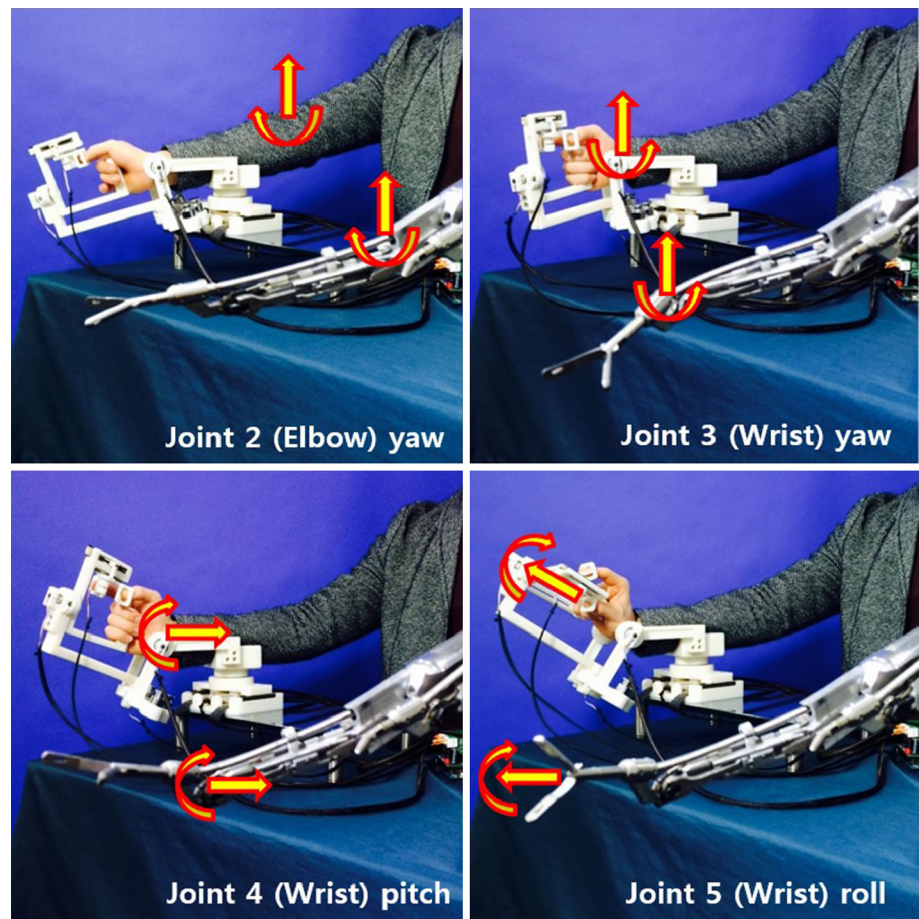


Fig. 11 Comparison of the trajectories of joint 2 between the master and slave

while avoiding the mechanical errors of the slave robot. The Arduino electronics prototyping platform uploads the compiled firmware via a universal serial bus (USB) connection. The encoder values of the master device were obtained using a serial peripheral interface (SPI) connection. The joint

angles calculated by the encoder values were then multiplied by the mapping factors for each joint to determine the pose of the virtual slave robot.

To compare the trajectories of the tips of the master and the virtual slave, four rotational joints of the real mas-

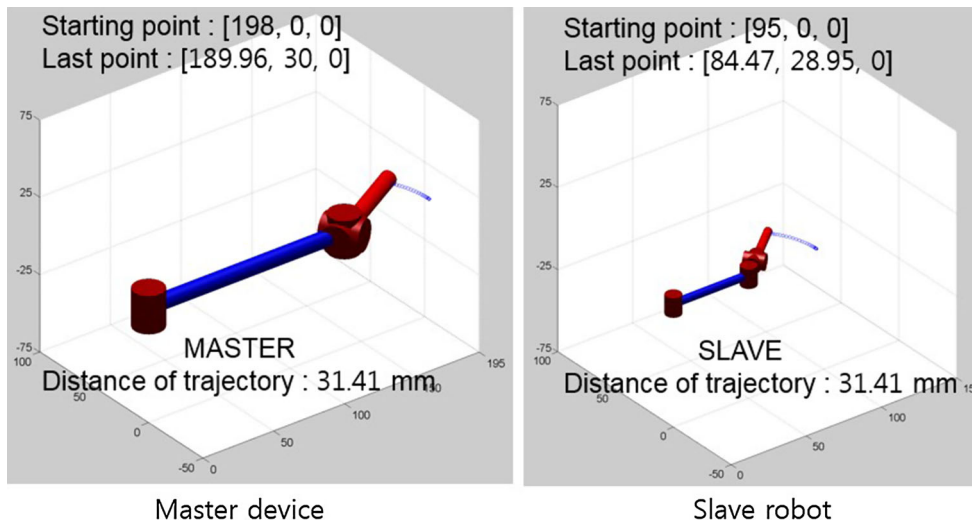


Fig. 12 Comparison of the trajectories of joint 3 between the master and slave

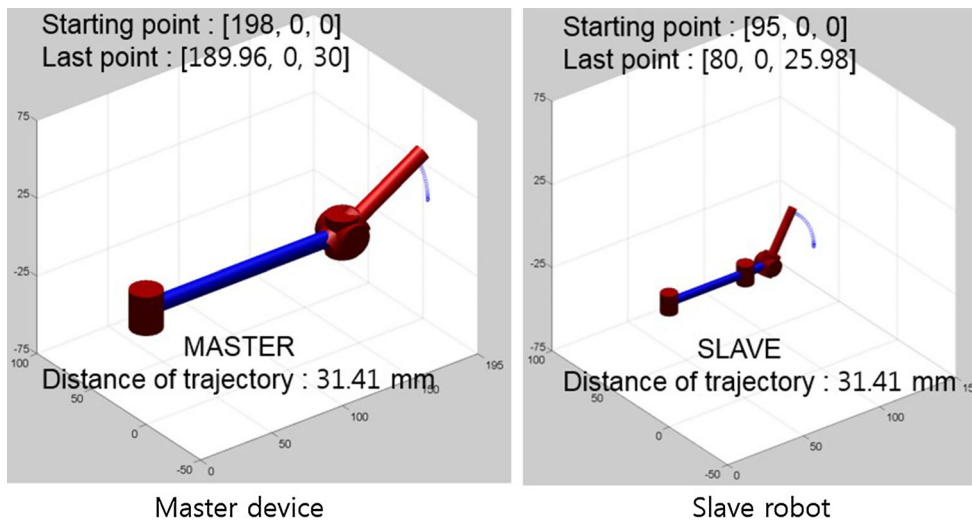


Fig. 13 Comparison of the trajectories of joint 4 between the master and slave

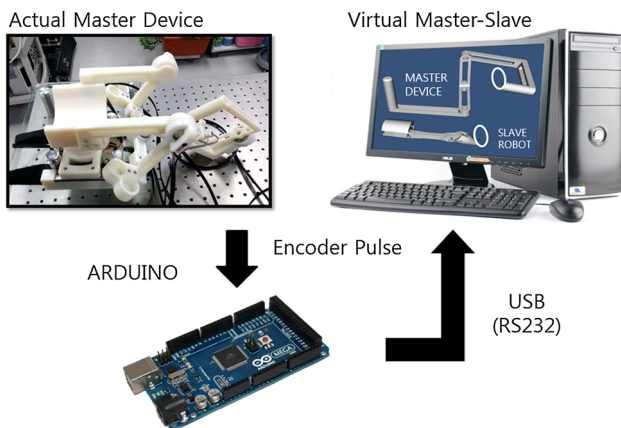


Fig. 14 Simulation system used to characterize the trajectory of the master device and slave robot

ter device were arbitrarily manipulated, and the trajectories were obtained. We confirmed that when the master device was manipulated five times, the trajectory error between the master and slave averaged 4%. Figure 15 shows a set of simulation results with a trajectory error of approximately 8 mm in 202 mm. However, the shapes and overall lengths of the trajectories of the master and slave were similar. We discuss the discrepancies and a solution for them in the following section.

Discussion

To implement master–slave operation in SPLS, we matched the human arm, the master, and the slave, while decoupling

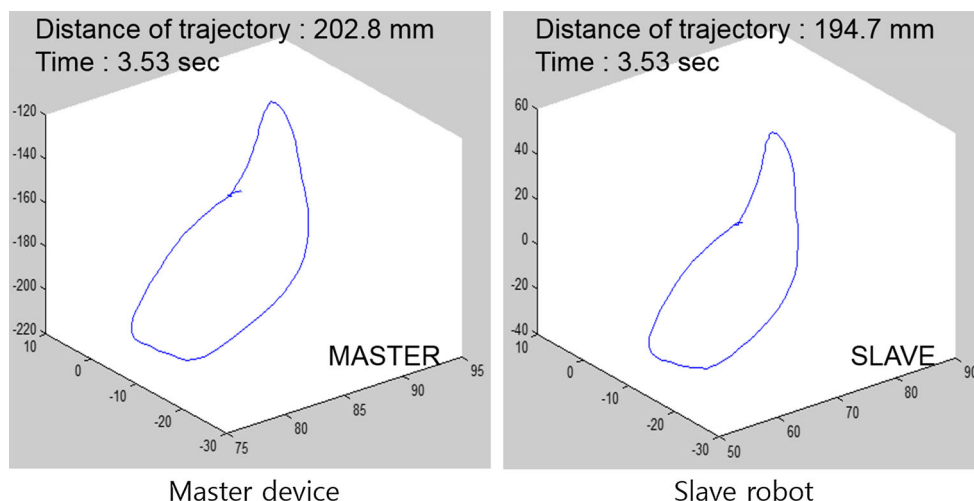


Fig. 15 Comparison of trajectories between the master and the virtual slave with four rotational joints

all of the joints. Decoupling is required to avoid possible collisions between the intermediate joints of the robot and tissue, as well as the endoscope. To obtain the desired tip motion of the slave, we determined appropriate mapping factors based on a kinematic analysis. Although the first simulation using MATLAB yielded identical trajectories of the joints when manipulated individually, when the joints move in combination, differences in the structures of the master and slave resulted in differences in the motions of the tips of the master and slave. Using Eqs. (11)–(14), we found that the velocity components v_y and v_z at the tips of the master and slave were equal but that the v_x velocity components differed. We detected a 4% trajectory error in the experiment, but this error can be overcome by a surgeon using visual feedback. If the robot must follow the exact trajectory planned prior to surgery, as in needle insertion into a small tumor, any small discrepancy between trajectories may cause serious problems. However, with SPLS, surgeons typically operate the master manually with visual feedback from the laparoscopic monitor. If the distance to the target can be estimated from the laparoscopic image, the surgeon may alter the trajectory of the master to reach the target. We can reduce this 4% error to almost 0% at the tip if we use the conventional inverse Jacobian approach. However, we cannot control other joints inside the body except the tip part. Therefore, 4% was inevitable error that we had to accept to control every joint inside the body for safety, as well as the tip part for the master–slave systems that have different structures from each other.

Berkelman et al. [22] also reported that using a master–slave system for a gripper reduced the trajectory error compared with manual operation. They showed that manual operation had more than 50% trajectory error, and even the reduced error was more than 10%. Considering these results, 4% error may be acceptable, or at least is much smaller than the error in manual operation.

Also, to determine each link length of the master device, the average length of human arms and size of hands were considered. In order to make the master device fit various operators' arms and hands, the component size should be made adjustable to each operator.

Conclusions

We designed a master device to support SPLS robots. In contrast to the da Vinci system, we chose all-joint control for the safe motion of the single-port surgery slave robot. We matched each joint of the master, the slave, and the human arm, while decoupling all-joint motions of the slave robot. Mapping factors were determined based on kinematic analysis and were used to achieve all-joint control with minimal error at the tip of the slave robot.

Acknowledgments This work was supported by the R&D Program of the DGIST Convergence Science Center (12-BD-0402).

Compliance with ethical standards

Conflict of interest The authors declare that they have no conflict of interest.

References

1. Chamberlain RS, Sakpal SV (2009) A comprehensive review of single-incision laparoscopic surgery (SILS) and natural orifice transluminal endoscopic surgery (NOTES) techniques for cholecystectomy. *J Gastrintest Surg* 13:1733–1740
2. Veldkamp R, Kuhry E, Hop W, Jeekel J, Kazemier G, Bonjer HJ, Haglind E, Pahlman L, Cuesta MA, Msika S, Morino M, Lacy AM (2005) Laparoscopic surgery versus open surgery for colon cancer: short-term outcomes of a randomised trial. *Lancet Oncol* 6:477–484

3. Kaouk JH, Goel RK, Haber GP, Crouzet S, Stein RJ (2009) Robotic single-port transumbilical surgery in humans: initial report. *BJU Int* 103:366–369
4. Autorino R, Cadeddu JA, Desai MM, Gettman M, Gill IS, Kavoussi LR, Lima E, Montorsi F, Richstone L, Stolzenburg JU, Kaouk JH (2011) Laparoendoscopic single-site and natural orifice transluminal endoscopic surgery in urology: a critical analysis of the literature. *Eur Urol* 59:26–45
5. Cindolo L, Gidaro S, Tamburro FR, Schips L (2010) Laparoendoscopic single-site left transperitoneal adrenalectomy. *Eur Urol* 57:911–914
6. Lanfranco AR, Castellanos AE, Desai JP, Meyers WC (2004) Robotic surgery: a current perspective. *Ann Surg* 239:14
7. Howe RD, Matsuoka Y (1999) Robotics for surgery. *Annu Rev Biomed Eng* 1:211–240
8. Haber GP, White MA, Autorino R, Escobar PF, Kroh MD, Chalikonda S, Khanna R, Forest S, Yang B, Altunrende F, Stein RJ, Kaouk JH (2010) Novel robotic da Vinci instruments for laparoendoscopic single-site surgery. *Urology* 76:1279–1282
9. Autorino R, Kaouk JH, Stolzenburg JU, Gill IS, Mottrie A, Tewari A, Cadeddu JA (2013) Current status and future directions of robotic single-site surgery: a systematic review. *Eur Urol* 63:266–280
10. Silva AJ, Ramirez OAD, Vega VP, Oliver JPO (2009) Phantom omni haptic device: kinematic and manipulability. In: electronics, robotics and automotive mechanics conference CERMA'09:193–198
11. Hagn U, Konietzschke R, Tobergte A, Nickl M, Jörg S, Kübler B, Passig G, Gröger M, Fröhlich F, Seibold U, Le-Tien L, Albuschäffer A, Nothhelfer A, Hacker F, Grebenstein M, Hirzinger G (2010) DLR MiroSurge: a versatile system for research in endoscopic telesurgery. *Int J Comp Assist Radiol Surg* 5:183–193
12. Tadakuma R, Asahara Y, Kajimoto H, Kawakami N, Tachi S (2005) Development of anthropomorphic multi-DOF master–slave arm for mutual teleexistence. *IEEE Trans Vis Comput Graph* 11:626–636
13. Ikuta K, Hasegawa T, Daifu S (2003) Hyper redundant miniature manipulator “Hyper Finger” for remote minimally invasive surgery in deep area. In: Proceedings of IEEE conference on robotics and automation, ICRA'03. pp 1098–1102
14. Thant Z, Low S, Tang S, Phee L, Ho K, Chung S (2006) Ergonomic master controller for flexible endoscopic gastrointestinal robot manipulator. In: International conference on biomedical and pharmaceutical engineering ICBPE, 2006, pp 575–579
15. Phee SJ, Low SC, Huynh V, Kencana AP, Sun Z, Yang K (2009) Master and slave transluminal endoscopic robot (MASTER) for natural orifice transluminal endoscopic surgery (NOTES). In: IEEE annual international conference on engineering in medicine and biology society, 2009, pp 1192–1195
16. Cheon B, Gezgin E, Ji DK, Tomikaw M, Hashizume M, Kim HJ, Hong JS (2014) A single port laparoscopic surgery robot with high force transmission and a large workspace. *Surg Endosc* 28:2719–2729
17. Wang X (1999) A behavior-based inverse kinematics algorithm to predict arm prehension postures for computer-aided ergonomic evaluation. *J Biomech* 32:453–460
18. Perry JC, Rosen J, Burns S (2007) Upper-limb powered exoskeleton design. *IEEE/ASME Trans Mech* 12:408–417
19. Hayward V, Gregorio P, Astley O, Greenish S, Doyon M, Lessard L, McDougall J, Sinclair I, Boelen S, Chen X, Demers JG, Poulin J, Benguigui I, Almey N, Makuc B, Zhang X (1998) Freedom-7: a high fidelity seven axis haptic device with application to surgical training. In: Casals A, de Almeida AT (eds) *Experimental robotics V*. Springer, Heidelberg, pp 443–456
20. Craig JJ (2005) *Introduction to robotics: mechanics and control*, Chapter 5. Pearson Prentice Hall, Upper Saddle River, vol 3, pp 135–164
21. Craig JJ (2005) *Introduction to robotics: mechanics and control*, Chapter 3. Pearson Prentice Hall, Upper Saddle River, vol 3, pp 62–100
22. Berkelman P, Ma J (2009) A compact modular teleoperated robot system for laparoscopic surgery. *Int J Robot Res* 28:1198–1215